Surface-Mediated Two-Dimensional Growth of the Pharmaceutical Carbamazepine

Erin V. Iski,[†] Blair F. Johnston,[‡] Alastair J. Florence,[‡] Andrew J. Urquhart,[‡] and E. Charles H. Sykes[†,*]

[†]Department of Chemistry, Pearson Chemistry Laboratory, Tufts University, Medford, Massachusetts 02155-5813 and [‡]Strathclyde Institute of Pharmacy and Biomedical Sciences, University of Strathclyde, The John Arbuthnott Building, 27 Taylor Street, Glasgow G4 0NR, U.K.

ARTICLE

ABSTRACT Scanning tunneling microscopy (STM) has become a staple surface microscopy technique for a number of research fields ranging from semiconductor research to heterogeneous catalysis. Pharmaceutical compounds, however, remain largely unstudied. Here we report the first STM study of carbamazepine (CBZ), an anti-epileptic drug, on Au(111) and Cu(111) surfaces. The analysis reveals that CBZ adopts unusual chiral molecular architectures on both metals. These previously unreported structures, which are strikingly different from CBZ packing arrangements observed in 3D crystal structures, indicate that the main molecular architecture is driven by a combination of CBZ intermolecular hydrogen bonding and metal—CBZ interactions. Comparison of the 2D molecular structures reveals large differences in local geometry and packing density that are dependent on the nature of the metal surface. These results have implications for the potential role of metal surfaces as heteronuclei or templating agents for controlling polymorph formation, which continues to be a problem for many compounds in the pharmaceutical industry including CBZ.

KEYWORDS: carbamazepine · polymorph · heteronuclei · surface · STM

Since the advent of scanning tunneling microscopy (STM) as a surface probe technique in the 1980s, a wide range of molecules on various surfaces have been investigated to reveal detail at the nanoscale.[1,2] These studies have covered scientific fields as diverse as semiconductor research[3] to heterogeneous catalysis,[4] with biological macromolecules also receiving some attention.[5] One field of study that has remained relatively unexplored is that of pharmaceutical drug molecules adsorbed on surfaces.[6] Typically, another scanning probe technique, atomic force microscopy (AFM),[6] has been used to investigate the structure and properties of such systems. Hence, the only published work to date using STM in this area has focused on the study of self-assembled monolayers of thiolated paracetamol and benzocaine derivatives[7] rather than on pure drug molecules. This is perhaps surprising given the potential for STM to explore the nanoscale mechanism of drug adsorption and crystal growth on metal surfaces.

Polymorphism (*i.e.*, crystallization into different packing arrangements) is a substantial problem for the pharmaceutical industry as different polymorphs of the same compound must be rigorously characterized and controlled due to their different physical properties. Heteronuclei or surfaces that aid nucleation are known to influence polymorph specificity;[8] therefore, understanding the role of how heteronuclei surface properties influence polymorph specificity could ultimately lead to rational polymorph selection, where heteronuclei are specifically chosen to produce particular polymorphic structures, in stark contrast to the largely empirical approach currently used in high-throughput polymorph screening. Drug molecule polymorphs are particularly problematic as different crystal forms can show significant differences in key physical properties, impacting large-scale industrial manufacturing and potentially resulting in altered bioavailability of dosage forms.[9]

While STM can afford access to exceptionally detailed molecular packing information, pharmaceutical molecules present many difficulties when studied with this technique, such as low vapor pressure and chemical lability that can hinder sample preparation, particularly in the ultrahigh vacuum (UHV) applications considered here. In addition to these practical challenges in sample preparation, image analysis of STM data consisting of organic molecules, which possess the conformational flexibility and diverse chemical functionalities characteristic of typical drug compounds, is also challenging. While the identification of rigid polycyclic aromatic compounds (*e.g.*, tetracene, porphyrin rings, *etc.*) can often be achieved by facile superimposition of two-dimensional molecular models over the electron density lobes

*Address correspondence to charles.sykes@tufts.edu.

Received for review April 23, 2010 and accepted August 24, 2010.

Published online September 2, 2010. 10.1021/nn100868r

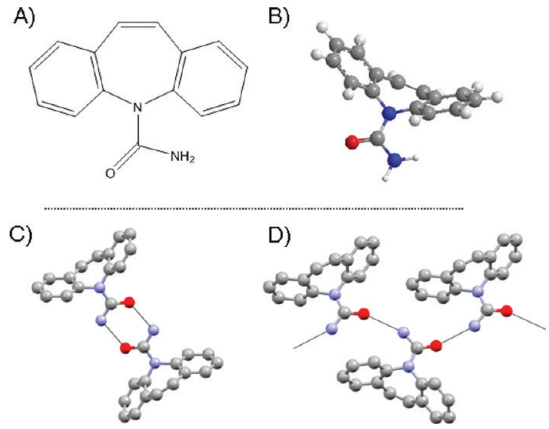

Figure 1. Structural models of carbamazepine (CBZ). (A) Two-dimensional molecular structure. (B) Three-dimensional *in vacuo* geometry optimized structure of CBZ showing the "butterfly-like" geometry. (C) Experimentally observed pairwise interaction that dominates 3D CBZ crystal polymorphs. (D) Additional stable association geometry predicted for 3D CBZ packing.[40]

presented in the STM image,[10−13] image analysis becomes less straightforward when the molecules adsorb in nonplanar configurations.[14−18] This latter issue becomes particularly critical if STM is to be used for the analysis of extended arrays/motifs of complex supramolecular assemblies often implicated in nanotechnology.[19−39]

In this publication, we describe the molecular arrangements of a well-studied, commercially available drug molecule, carbamazepine (CBZ)[40] (Figure 1) on Au(111) and Cu(111) metal surfaces in UHV. In contrast to the pairwise interactions observed in 3D crystal structures of CBZ (Figure 1C), we report a previously unseen CBZ trimer packing motif on both metal surfaces, which highlights the hydrogen bonding induced stability of the surface-bound trimer. Metal−CBZ electron overlap has a critical influence on the complex 2D molecular architectures formed by packing the CBZ trimers, with both metal surfaces inducing organizational chirality[41] in the molecular architectures, albeit in different ways. On Au(111), homochiral domains of CBZ trimers are observed resulting in a 2D conglomerate where ultimately there is a racemic mixture of chiral domains (similar to 3D crystal conglomerates which are racemic mixtures composed of physically separated enantiopure domains).[42] Conversely, on Cu(111), heterochiral domains are formed with enantio-favoritism. These heterochiral domains are more densely packed than the homochiral domains observed on Au(111) and indicate that the heterochiral packing of CBZ trimers on Cu(111) is a more efficient packing approach and a 2D analogy of Wallach's rule from 1895, which states that racemic crystals tend to be denser than their enantiomerically pure counterparts.[43]

RESULTS AND DISCUSSION

CBZ was dosed onto Au(111) and Cu(111) single-crystal surfaces at coverages ranging from 0.02 to <1 ML at 78 K. In this case, a monolayer (ML) refers to a single layer of closely packed molecules. Miniature (2×2 mm^2) Au and Cu single crystals were mounted on the same sample plate so that experiments could be conducted in parallel. This ensured no variation in molecular dose or annealing temperature between the two surfaces. In order to avoid complexity arising from the crowding of molecules and distortion of packing, the coverage of CBZ on the surface was kept to approximately 0.5 ML. Figure 2 shows a ~0.5 ML coverage of CBZ on Au(111) and Cu(111) at 78 K with the CBZ molecules self-assembling to form large, ordered islands in which individual molecules pack with an apparent three-fold symmetry. The islands are surrounded by smaller CBZ clusters and individual molecules. Molecular vacancies are also observed in the 2D crystalline islands on both the Au(111) and Cu(111) surfaces, although vacancies occur with a greater frequency on Au (Figure 2). Other packing irregularities are also present on the Au surface, which are not observed on the Cu, and are therefore likely due to the underlying herringbone reconstruction of the Au(111) substrate. However, the basic, repeating packing unit observed across the majority of the two surfaces appears as a three-lobed structure (Figure 2), which is in stark contrast to the 3D structure of CBZ (Figure 1).

We propose that the three-lobed structures on both Au and Cu can be attributed to one of two types of trimers present on the surface, either a trimer formed by three hydrogen-bonded CBZ molecules ("CBZ trimer") or a trimer formed by intersecting dibenzazepine moieties of neighboring CBZ molecules ("dibenzazepine trimer"). The two types of trimers (Figure 3) are different in size with the sides of each equilateral triangle measuring ~8 Å for the CBZ trimer and ~6 Å for the dibenzazepine trimer on Au(111). Each molecule in the CBZ trimer (as seen in Figure 3) is orientated in such a way that both the amide group and one aromatic ring of the dibenzazepine moiety are in close contact with the metal surface, while the remaining aromatic ring points away from the surface. This tilted ring (which shall now be referred to as the "sail" ring) tilts away from the surface by a calculated angle of ~53°. In turn, the amide groups of the CBZ trimer adopt a three-fold symmetry, allowing favorable hydrogen bonding interactions between the adjacent amide groups. Because the sail ring of each CBZ molecule within the trimer is tilted slightly off of the surface, adjacent molecules are able to approach at a closer distance. Thus, each trimer configuration is formed from a concerted arrangement of individual CBZ molecules that also results in organizational chirality,[41] which can be reversed by switching which ring is in contact with the surface in each of the three CBZ molecules. The dibenzazepine trimers also

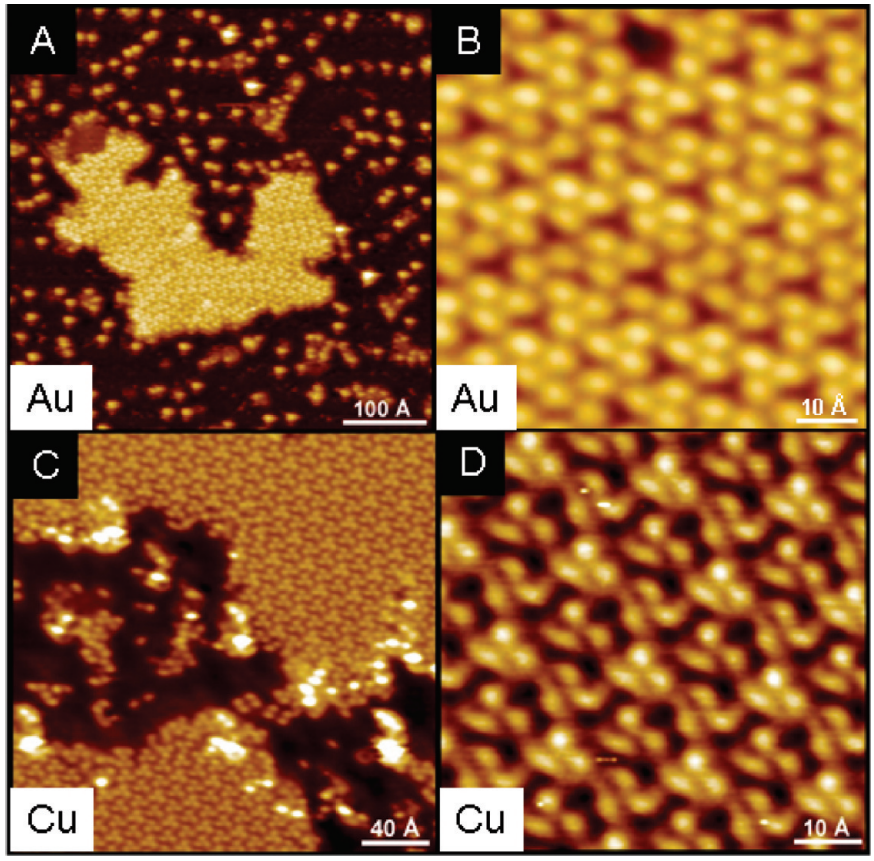

Figure 2. Formation of CBZ islands on Au(111)/ Cu(111). (A) On Au(111), the CBZ molecules form large, ordered islands as seen in this 500 × 500 Å^2 STM image (tunneling parameters: sample voltage (V_s) = −0.9 V, current (I) = 10 pA). (B) Ordering of the CBZ molecules within the island manifests with a unique three-lobed structure as evident in this molecularly resolved STM image. Some defects in the island due to missing molecules can also be seen (V_s = −1.2 V, I = 40 pA). (C) Similar to the packing arrangement on Au(111), CBZ forms large, ordered islands on Cu(111). In this 250 × 250 Å^2 STM image, it is possible to see two ordered islands beginning to merge (V_s = −1.2 V, I = 10 pA). (D) Interestingly, CBZ also adopts a trimer motif on the Cu surface as seen in this molecularly resolved STM image (V_s = −1 V, I = 30 pA).

have an associated chirality, which will be described in the following sections.

Figure 4A shows the energy minimized (with respect to atomic coordinates) model of the hydrogen-bonded trimer of CBZ on Au(111) as described above, with the sail ring highlighted in white. Applying a Connolly surface[44] (described in detail below) to this ball and stick model results in a trimer structure (Figure 4B),

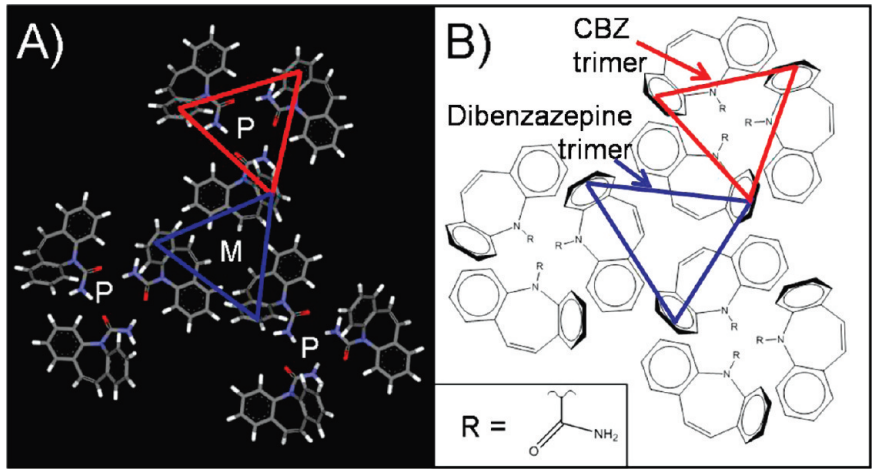

Figure 3. Organizational chirality and identity of trimers on Au(111). (A) Energy minimized model of three CBZ trimers on Au(111) (surface not shown for clarity). The red triangle designates a CBZ trimer, while the blue triangle designates a dibenzazepine trimer. The chiral configuration of each trimer due to the directionality of the tilted rings is denoted by a white letter, either "P" or "M". The chiral assignment is unconnected with the trimer's identity, and each type of trimer can be of either chirality. (B) Schematic of three CBZ trimers for clarification with the identity of the trimers indicated.

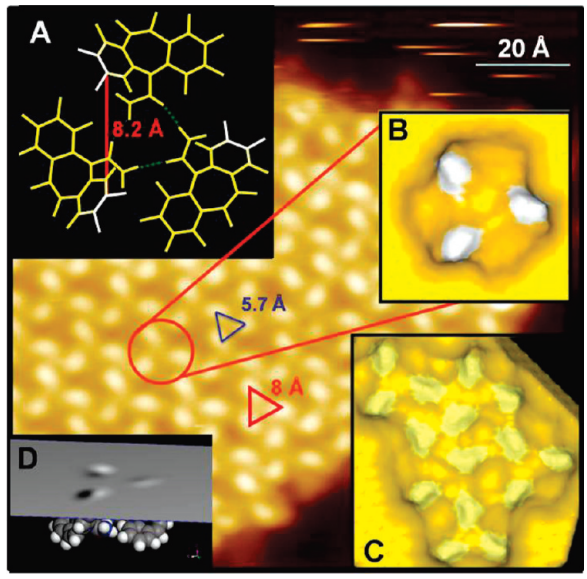

Figure 4. Connolly surface of CBZ arrangement. (A) Energy minimized model trimer of CBZ on Au(111) indicating how the molecules must tilt in order to arrange and form hydrogen bonds (surface not shown for clarity). (B) Connolly surface model of the region of the STM image encircled in red (V_s = −1.2 V, I = 5 pA). Not only does the model visually complement the STM images, but the dimensions of the model follow those of the images, as well. (C) When examining the packing of multiple trimers as described by the Connolly model, it is notable that the model packing matches the arrangement in the STM images. (D) A slice through the periodic cell, coplanar with the Au surface and level with the top of the CBZ trimer, shows the electron density of the HOMO. The two triangles in the central STM image show approximate dimensions for the CBZ trimer (highlighted in red) and the dibenzazepine trimer (highlighted in blue).

which is very similar in appearance to the observed three-lobed features in the STM images. Moreover, this can be extended by 2D translation to yield an array that significantly resembles the extended islands visible in the STM data (Figure 4C). The Connolly surfaces suggest that the lobes of maximum intensity in the STM images correspond to the tips of the sail rings of the three CBZ molecules within the CBZ trimer. As the STM images display the height of the tip as it raster scans across the sample with a constant tunneling current, it is worth considering the physical meaning of the Connolly surface in this context.

The Connolly surface,[44] also called solvent excluded surface, provides a means to visualize the accessibility of a molecular surface to a probe. This type of modeling is most commonly used to model protein surfaces where the probe is a sphere of water (usually 1.4 Å in radius).[44] However, surface modeling approaches which utilize probes can in theory be applied to STM images with the probe representing the STM tip rather than a solvent. All currents used for imaging were on the order of picoamps and, therefore, represent nonperturbative scanning conditions at which the STM tip is not penetrating into the molecular film on the surface. A slice through the periodic cell, coplanar with the Au surface and level with the top of the CBZ trimer, which shows the electron density of the HOMO, can be seen in Figure 4D. This closely matches the highlighted upper regions of the Connolly surface, which would be most exposed to the STM tip. The trimer model also fits the observed dimensionality of the three-lobed structure observed in the STM images (Figure 4; see the ~8 × 8 × 8 Å red triangle). The problem of using a purely planar CBZ model to describe the three-lobed structure relates to the fact that a planar CBZ model would not fit the observed dimensions.

Furthermore, the butterfly geometry of CBZ (Figure 1B) in the gas phase closely matches the geometry observed in 3D crystals.[40] Taking the proposed CBZ trimer model, each amide group is now in an environment where it can not only chemisorb to the metal surface but also form a cyclic hydrogen-bonded motif with adjacent amide groups. Although arguably obvious, a semiempirical geometry optimization of a free trimer removed from the Au(111) surface shows that, although the trimer deforms when not constrained to planarity by the Au surface, the hydrogen bonding motif is retained in the optimized, isolated arrangement. The trimer arrangement also allows the aromatic groups lying parallel to the surface to form π-metal interactions, which further stabilize the overall arrangement.

This novel molecular architecture represents a mode of self-association for CBZ that is not observed in any of the known polymorphs[40] or in over the 50 multicomponent three-dimensional crystal structures reported to date in the Cambridge Structural Database.[45,46] As previously shown (Figure 3), each trimer motif has an associated chirality which derives from the sail ring of the dibenzazepine moiety. By extending the CBZ trimer motif through 2D translation to incorporate three CBZ trimers and computationally modeling the energy minimized system on Au(111) produces Figure 3A.

Here, each CBZ trimer motif adopts a P configuration, while the dibenzazapine trimer adopts the opposite M configuration. P and M are the chirality descriptors equivalent to R and S but in the helical definition of chirality appropriate for the trimer structures observed here.[47] As stated previously, the classification of chirality and trimer identity are not directly related. Each type of trimer can be of either chirality. Molecular chirality on metal surfaces has been reported for a number of systems[14,48−53] and can be attributed to either locally breaking substrate symmetry through molecular adsorption (conformational and point chirality) or from the tilting of molecular structures (organizational chirality) as observed with CBZ on Au and Cu surfaces.[41] On Au(111), domains of CBZ trimers with specific chiral configurations are produced, as shown in Figure 5. These domains are homochiral, regardless of chiral perspective, in that all CBZ trimers within a domain will have one configuration while all dibenzazepine trimers within the domain will have the opposite chiral configuration (*e.g.*, a P domain of CBZ trimers corresponds to a

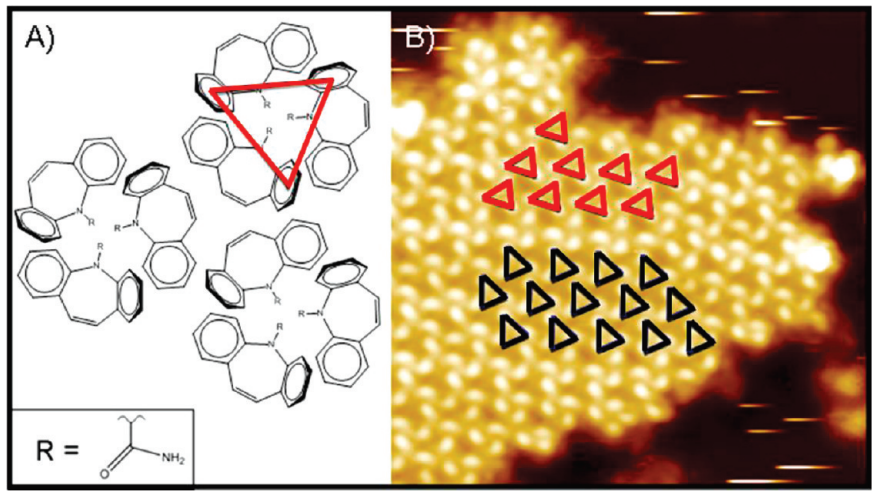

Figure 5. Homochiral CBZ domains on Au(111). (A) Schematic diagram of three CBZ trimers where each CBZ trimer has a P configuration (shown by the red triangle). (B) STM image of CBZ on Au(111) showing the two different homochiral domains of the CBZ trimers (red triangles denote a P configuration, while black triangles denote a M configuration).

M domain of dibenzazepine trimers). It is even possible to analyze each image and assign approximate percentages of P and M configurations (Figure 5B). Overall, across a number of CBZ domains on Au(111) (not shown), the ratio of P to M configurations (whether comparing CBZ trimers or dibenzazepine trimers) is approximately 50:50 (±10%). Domain homochirality and resulting global racemic mixtures have been previously reported for a number of systems on metal surfaces.[54−58] In regard to the appearance of the adsorbates near the edges of the island in Figure 5, it is well understood that adsorbates at island edges may appear differently in STM images due to a different interaction of the STM tip with the higher aspect ratio edge *versus* the flatter surface of the island. The side of the STM tip contributes to the topographic contour of the edge, and features can appear distorted. Furthermore, the ordering of the adsorbates breaks down near the edges of the islands due to a lack of neighboring molecules, leading to different local orientations of the edge molecules.

The Cu(111) surface alters the CBZ domain structure to produce a highly packed mixture of M and P trimers as opposed to the simpler homochiral three-fold symmetry observed on Au(111). This molecular packing approximates to 2.7 CBZ molecules/nm^2 on Cu compared with approximately 1.7 CBZ molecules/nm^2 observed on Au. Each three-lobed structure observed on Cu is dimensionally too small to be attributed to the CBZ trimer observed on Au (*i.e.*, 5 × 5 × 5 Å compared with 8 × 8 × 8 Å). Instead, the three-lobed structures can be attributed to the dibenzazepine trimer (Figure 6), which is more closely packed on the Cu surface than on the Au (Figures 3 and 5). Due to the geometry of the trimers and the way in which the tip images them on the surface, the lobes of the dibenzazepine trimer appear as nearest neighbors and the lobes of the CBZ trimer are more separated. Similar to CBZ on Au, each dibenzazepine trimer possesses organizational chirality with the six-fold symmetry being described as six P trimers with a central M trimer (2:1 P to M chiral ratio), which overall produces a hexagonal array. The fact that CBZ on Cu(111) appears to show local enantiofavoritism and has a far higher packing density than on Au(111) indicates that the heterochiral packing of CBZ on Cu produces a higher degree of packing than homochiral packing on Au.

Interestingly, the fact that the heterochiral CBZ domains on Cu(111) have a significantly higher packing density than the homochiral CBZ domains on Au(111) indicates that CBZ on Cu and Au surfaces obeys a 2D version of Wallach's rule (1895), which states that race-

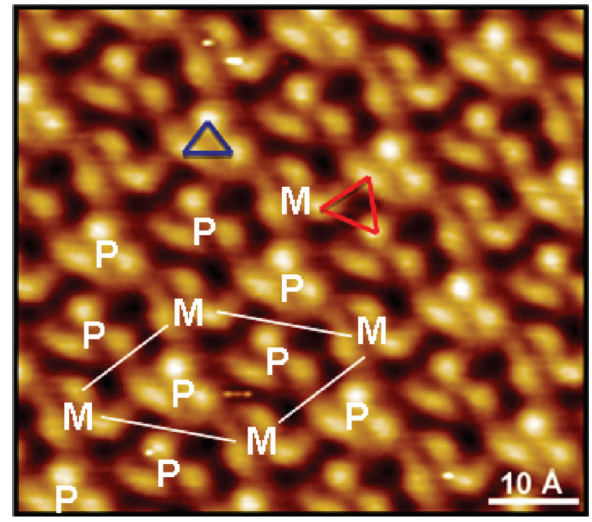

Figure 6. Heterochiral CBZ domains on Cu(111). STM image showing the hexagonal packing of CBZ on Cu(111). The two types of trimers present on Cu are shown, with the dibenzazepine trimer (highlighted in blue) and the CBZ trimer (highlighted in red). The heterochirality of the CBZ packing is shown using the dibenzazepine trimers (P and M white lettering). The white parallelogram indicates the basic unit cell of CBZ on Cu.

mically pure crystals tend to be denser than their enantiomerically pure counterparts.[43,59]

CONCLUSIONS

CBZ adsorption on Au and Cu(111) single crystals resulted in the formation of complex chiral molecular architectures that are previously unreported. The results presented here indicate that the architecture is governed by a number of phenomena that include (1) the potential of surface-bound CBZ molecules to form stable three-fold hydrogen-bonded motifs *via* the amide groups; (2) the ability of CBZ molecules to form close-packed trimer arrangements around the dibenzazepine moiety, enabling hydrogen-bonded trimer units to form densely packed arrays; and (3) interactions between the dibenzazepine and amide moieties of CBZ and the underlying metal surface. These architectures highlight the complexity of metal−drug molecule interactions but hint that metal surfaces may serve as heteronuclei for directing polymorph formation. As formation of one polymorph over another is often a subtle kinetic effect, sublimation of compounds onto different metal surfaces may provide a method to select a desired structure. The drastic difference between Cu and Au surface-supported 2D CBZ crystals demonstrates that the nature of the metal has a strong influence on the initial stages of crystal growth. The work also demonstrates the potential of STM as a technique for probing 2D drug molecular architectures and the relationship between molecular conformation, noncovalent intermolecular interactions, and extended structure. However, considerable work is still required to understand if complex 2D molecular architectures can be reliably utilized as templates to form novel 3D crystalline entities.

METHODS

Sample Preparation. The sample preparation and STM imaging were conducted in a LT-UHV Omicron NanoTechnology system that was cooled to 78 K with a base pressure $<5 \times 10^{-10}$ mbar. The Au(111) and Cu(111) single crystals (MaTeck) were cleaned prior to CBZ (99%, Sigma-Aldrich) deposition by cycles of Ar^+ sputtering (1.0 keV/18 μA) followed by thermal anneals to 1000 K. The cleanliness of the metal surfaces was verified with STM imaging. The substrates were kept at 78 K during molecular deposition and all STM imaging. The CBZ was heated to ~413 K and dosed onto the cold surfaces *via* sublimation into the STM chamber through a heated gas line and precision leak valve. The molecules were deposited on the samples through a collimated molecular doser. After dosing, the substrates were annealed to ~120 K.

Scanning Tunneling Microscopy. Topographic STM imaging was operated under the constant-current mode with the bias applied to the sample. All images were recorded with cut Pt/Ir wire tips (80/20, 0.25 mm diameter).

Surface Modeling. A model of three CBZ molecules adopting a H-bonded trimer motif with C_3 symmetry was generated to reflect the three-lobed patterns present in the STM images. This trimer was placed on a Au(111) surface, four atoms deep, and then added to a periodic cell (a = 28.8 Å, b = 28.8 Å, c = 30.0 Å, α = 90.0°, β = 90.0°, γ = 120.0°) with the Au surface perpendicular to the c-axis. The contents of the cell were then optimized without symmetry constraints using DMol3[60] with the PW91 functional[61] and DNP (double numerical plus polarization) basis set, using DFT semicore pseudopotentials.[62] A single k-point was used along with an SCF convergence tolerance of $1.0e^{-5}$ Ha, and both HOMO and LUMO MO densities for the final structure were calculated. The optimized trimer was then replicated to allow a close-packed arrangement between three trimers that could be further investigated. In this instance, the Au surface was six atoms deep, and the periodic cell dimensions were increased (a = 57.7 Å, b = 57.7 Å, c = 50.0 Å, α = 90.0°, β = 90.0°, γ = 120.0°) to accommodate the larger system. Geometry optimization was carried out with Accelrys' Discover with the COMPASS force field[63] using the BFGS minimizer and a 0.001 kcal mol^{-1} $Å^{-1}$ convergence criteria.

Acknowledgment. C.S. and E.I. thank the National Science Foundation, the Beckman Foundation and Research Corporation for support. E.I. acknowledges the Department of Education for a GAANN fellowship.

REFERENCES AND NOTES

1. De Feyter, S.; De Schryver, F. C. Two-Dimensional Supramolecular Self-Assembly Probed by Scanning Tunneling Microscopy. *Chem. Soc. Rev.* **2003**, *32*, 139–150.
2. Hansma, P. K.; Elings, V. B.; Marti, O.; Bracker, C. E. Scanning Tunneling Microscopy and Atomic Force Microscopy—Application to Biology and Technology. *Science* **1988**, *242*, 209–216.
3. Kubby, J. A.; Boland, J. J. Scanning Tunneling Microscopy of Semiconductor Surfaces. *Surf. Sci. Rep.* **1996**, *26*, 61–204.
4. Vang, R. T.; Lauritsen, J. V.; Laegsgaard, E.; Besenbacher, F. Scanning Tunneling Microscopy as a Tool To Study Catalytically Relevant Model Systems. *Chem. Soc. Rev.* **2008**, *37*, 2191–2203.
5. Shapir, E.; Yi, J. Y.; Cohen, H.; Kotlyar, A. B.; Cuniberti, G.; Porath, D. The Puzzle of Contrast Inversion in DNA STM Imaging. *J. Phys. Chem. B* **2005**, *109*, 14270–14274.
6. Tumer, Y. T. A.; Roberts, C. J.; Davies, M. C. Scanning Probe Microscopy in the Field of Drug Delivery. *Adv. Drug Delivery Rev.* **2007**, *59*, 1453–1473.
7. Popoff, A.; Fichou, D. Immobilization of Paracetamol and Benzocaine Pro-Drug Derivatives as Long-Range Self-Organized Monolayers on Graphite. *Colloids Surf., B* **2008**, *63*, 153–158.
8. Lang, M. D.; Grzesiak, A. L.; Matzger, A. J. The Use of Polymer Heteronuclei for Crystalline Polymorph Selection. *J. Am. Chem. Soc.* **2002**, *124*, 14834–14835.
9. Rustichelli, C.; Gamberini, G.; Ferioli, V.; Gamberini, M. C.; Ficarra, R.; Tommasini, S. Solid-State Study of Polymorphic Drugs: Carbamazepine. *J. Pharm. Biomed. Anal.* **2000**, *23*, 41–54.
10. Chen, Q.; McDowall, A. J.; Richardson, N. V. Ordered Structures of Tetracene and Pentacene on Cu(110) Surfaces. *Langmuir* **2003**, *19*, 10164–10171.
11. Clair, S.; Pons, S.; Seitsonen, A. P.; Brune, H.; Kern, K.; Barth, J. V. STM Study of Terephthalic Acid Self-Assembly on Au(III): Hydrogen-Bonded Sheets on an Inhomogeneous Substrate. *J. Phys. Chem. B* **2004**, *108*, 14585–14590.
12. Kato, N. A.; Hara, M.; Sasabe, H.; Knoll, W. An Interpretation for the STM Imaging of an Organic Molecule, Tetrathiafulvalene-Tetracyanoquinodimethane (Ttf-Tcnq). *Nanotechnology* **1996**, *7*, 122–127.
13. Williams, F. J.; Vaughan, O. P. H.; Knox, K. J.; Bampos, N.; Lambert, R. M. First Observation of Capping/Uncapping by a Ligand of a Zn Porphyrin Adsorbed on Ag(100). *Chem. Commun.* **2004**, 1688–1689.

14. Fasel, R.; Parschau, M.; Ernst, K. H. Amplification of Chirality in Two-Dimensional Enantiomorphous Lattices. *Nature* **2006**, *439*, 449–452.
15. De Feyter, S.; De Schryver, F. C. Self-Assembly at the Liquid/Solid Interface: STM Reveals. *J. Phys. Chem. B* **2005**, *109*, 4290–4302.
16. Iancu, V.; Hla, S. W. Realization of a Four-Step Molecular Switch in Scanning Tunneling Microscope Manipulation of Single Chlorophyll-a Molecules. *Proc. Natl. Acad. Sci. U.S.A.* **2006**, *103*, 13718–13721.
17. Blum, M. C.; Pivetta, M.; Patthey, F.; Schneider, W. D. Probing and Locally Modifying the Intrinsic Electronic Structure and the Conformation of Supported Nonplanar Molecules. *Phys. Rev. B* **2006**, *73*, 195409.
18. Yokoyama, T.; Yokoyama, S.; Kamikado, T.; Mashiko, S. Nonplanar Adsorption and Orientational Ordering of Porphyrin Molecules on Au(111). *J. Chem. Phys.* **2001**, *115*, 3814–3818.
19. Theobald, J. A.; Oxtoby, N. S.; Phillips, M. A.; Champness, N. R.; Beton, P. H. Controlling Molecular Deposition and Layer Structure with Supramolecular Surface Assemblies. *Nature* **2003**, *424*, 1029–1031.
20. Kudernac, T.; Lei, S. B.; Elemans, J.; De Feyter, S. Two-Dimensional Supramolecular Self-Assembly: Nanoporous Networks on Surfaces. *Chem. Soc. Rev.* **2009**, *38*, 402–421.
21. Barth, J. V. Molecular Architectonic on Metal Surfaces. *Annu. Rev. Phys. Chem.* **2007**, *58*, 375–407.
22. De Feyter, S.; Miura, A.; Yao, S.; Chen, Z.; Wurthner, F.; Jonkheijm, P.; Schenning, A.; Meijer, E. W.; De Schryver, F. C. Two-Dimensional Self-Assembly into Multicomponent Hydrogen-Bonded Nanostructures. *Nano Lett.* **2005**, *5*, 77–81.
23. Furukawa, S.; Tahara, K.; De Schryver, F. C.; Van der Auweraer, M.; Tobe, Y.; De Feyter, S. Structural Transformation of a Two-Dimensional Molecular Network in Response to Selective Guest Inclusion. *Angew. Chem., Int. Ed.* **2007**, *46*, 2831–2834.
24. Stepanow, S.; Lingenfelder, M.; Dmitriev, A.; Spillmann, H.; Delvigne, E.; Lin, N.; Deng, X. B.; Cai, C. Z.; Barth, J. V.; Kern, K. Steering Molecular Organization and Host-Guest Interactions Using Two-Dimensional Nanoporous Coordination Systems. *Nat. Mater.* **2004**, *3*, 229–233.
25. Theobald, J. A.; Oxtoby, N. S.; Champness, N. R.; Beton, P. H.; Dennis, T. J. S. Growth Induced Reordering of Fullerene Clusters Trapped in a Two-Dimensional Supramolecular Network. *Langmuir* **2005**, *21*, 2038–2041.
26. Madueno, R.; Raisanen, M. T.; Silien, C.; Buck, M. Functionalizing Hydrogen-Bonded Surface Networks with Self-Assembled Monolayers. *Nature* **2008**, *454*, 618–621.
27. Gourdon, A. On-Surface Covalent Coupling in Ultrahigh Vacuum. *Angew. Chem., Int. Ed.* **2008**, *47*, 6950–6953.
28. Champness, N. R. Building with Molecules. *Nat. Nanotechnol.* **2007**, *2*, 671–672.
29. Sakamoto, J.; van Heijst, J.; Lukin, O.; Schluter, A. D. Two-Dimensional Polymers: Just a Dream of Synthetic Chemists. *Angew. Chem., Int. Ed.* **2009**, *48*, 1030–1069.
30. Perepichka, D. F.; Rosei, F. Chemistry Extending Polymer Conjugation into the Second Dimension. *Science* **2009**, *323*, 216–217.
31. Grill, L.; Dyer, M.; Lafferentz, L.; Persson, M.; Peters, M. V.; Hecht, S. Nano-Architectures by Covalent Assembly of Molecular Building Blocks. *Nat. Nanotechnol.* **2007**, *2*, 687–691.
32. Gutzler, R.; Walch, H.; Eder, G.; Kloft, S.; Heckl, W. M.; Lackinger, M. Surface Mediated Synthesis of 2D Covalent Organic Frameworks: 1,3,5-Tris(4-bromophenyl)benzene on Graphite(001), Cu(111), and Ag(110). *Chem. Commun.* **2009**, 4456–4458.
33. Weigelt, S.; Busse, C.; Bombis, C.; Knudsen, M. M.; Gothelf, K. V.; Strunskus, T.; Woll, C.; Dahlbom, M.; Hammer, B.; Laegsgaard, E.; Besenbacher, F.; Linderoth, T. R. Covalent Interlinking of an Aldehyde and an Amine on a Au(111) Surface in Ultrahigh Vacuum. *Angew. Chem., Int. Ed.* **2007**, *46*, 9227–9230.
34. Treier, M.; Richardson, N. V.; Fasel, R. Fabrication of Surface-Supported Low-Dimensional Polyimide Networks. *J. Am. Chem. Soc.* **2008**, *130*, 14054–14055.
35. Treier, M.; Fasel, R.; Champness, N. R.; Argent, S.; Richardson, N. V. Molecular Imaging of Polyimide Formation. *Phys. Chem. Chem. Phys.* **2009**, *11*, 1209–1214.
36. Jensen, S.; Fruchtl, H.; Baddeley, C. J. Coupling of Triamines with Diisocyanates on Au(111) Leads to the Formation of Polyurea Networks. *J. Am. Chem. Soc.* **2009**, *131*, 16706–16713.
37. Pawin, G.; Wong, K. L.; Kim, D.; Sun, D. Z.; Bartels, L.; Hong, S.; Rahman, T. S.; Carp, R.; Marsella, M. A Surface Coordination Network Based on Substrate-Derived Metal Adatoms with Local Charge Excess. *Angew. Chem., Int. Ed.* **2008**, *47*, 8442–8445.
38. Pawin, G.; Wong, K. L.; Kwon, K. Y.; Bartels, L. A Homomolecular Porous Network at a Cu(111) Surface. *Science* **2006**, *313*, 961–962.
39. Baro, A. M.; Hla, S. W.; Rieder, K. H. LT-STM Study of Self-Organization of β-Carotene Molecular Layers on Cu(111). *Chem. Phys. Lett.* **2003**, *369*, 240–247.
40. Florence, A. J.; Johnston, A.; Price, S. L.; Nowell, H.; Kennedy, A. R.; Shankland, N. An Automated Parallel Crystallisation Search for Predicted Crystal Structures and Packing Motifs of Carbamazepine. *J. Pharm. Sci.* **2006**, *95*, 1918–1930.
41. Bombis, C.; Weigelt, S.; Knudsen, M.; Nørgaard, M.; Busse, C.; Lægsgaard, E.; Besenbacher, F.; Gothelf, K. V.; Linderoth, T. R. Steering Organizational and Conformational Surface Chirality by Controlling Molecular Chemical Functionality. *ACS Nano* **2010**, *4*, 297–311.
42. Jaques, J.; Collet, A.; Wilen, S. H. *Enantiomers, Racemates and Resolutions*; Wiley: New York, 1981.
43. Brock, C. P.; Schweizer, W. B.; Dunitz, J. D. On the Validity of Wallach Rule—On the Density and Stability of Racemic Crystals Compared with Their Chiral Counterparts. *J. Am. Chem. Soc.* **1991**, *113*, 9811–9820.
44. Norel, R.; Lin, S. L.; Wolfson, H. J.; Nussinov, R. Shape Complementarity at Protein−Protein Interfaces. *Biopolymers* **1994**, *34*, 933–940.
45. Allen, F. H. The Cambridge Structural Database: A Quarter of a Million Crystal Structures and Rising. *Acta Crystallogr., Sect. B* **2002**, *58*, 380–388.
46. Allen, F. H.; Motherwell, W. D. S. Applications of the Cambridge Structural Database in Organic Chemistry and Crystal Chemistry. *Acta Crystallogr., Sect. B* **2002**, *58*, 407–422.
47. Eliel, E. L.; Wilen, S. H. *Stereochemistry of Organic Compounds*; John Wiley & Sons Inc.: New York, 1994.
48. Fang, H. B.; Giancarlo, L. C.; Flynn, G. W. Direct Determination of the Chirality of Organic Molecules by Scanning Tunneling Microscopy. *J. Phys. Chem. B* **1998**, *102*, 7311–7315.
49. Lorenzo, M. O.; Baddeley, C. J.; Muryn, C.; Raval, R. Extended Surface Chirality from Supramolecular Assemblies of Adsorbed Chiral Molecules. *Nature* **2000**, *404*, 376–379.
50. Parschau, M.; Fasel, R.; Ernst, K. H. Coverage and Enantiomeric Excess Dependent Enantiomorphism in Two-Dimensional Molecular Crystals. *Cryst. Growth Des.* **2008**, *8*, 1890–1896.
51. Liu, N.; Haq, S.; Darling, G. R.; Raval, R. Direct Visualization of Enantiospecific Substitution of Chiral Guest Molecules into Heterochiral Molecular Assemblies at Surfaces. *Angew. Chem., Int. Ed.* **2007**, *46*, 7613–7616.
52. Wei, Y. H.; Kannappan, K.; Flynn, G. W.; Zimmt, M. B. Scanning Tunneling Microscopy of Prochiral Anthracene Derivatives on Graphite: Chain Length Effects on Monolayer Morphology. *J. Am. Chem. Soc.* **2004**, *126*, 5318–5322.
53. Cai, Y. G.; Bernasek, S. L. Structures Formed by the Chiral Assembly of Racemic Mixtures of Enantiomers: Iodination Products of Elaidic and Oleic Acids. *J. Phys. Chem. B* **2005**, *109*, 4514–4519.
54. Kuhnle, A.; Linderoth, T. R.; Hammer, B.; Besenbacher, F.

Chiral Recognition in Dimerization of Adsorbed Cysteine Observed by Scanning Tunnelling Microscopy. *Nature* **2002**, *415*, 891–893.
55. Haq, S.; Liu, N.; Humblot, V.; Jansen, A. P. J.; Raval, R. Drastic Symmetry Breaking in Supramolecular Organization of Enantiomerically Unbalanced Monolayers at Surfaces. *Nat. Chem.* **2009**, *1*, 409–414.
56. Jiang, N.; Wang, Y.; Liu, Q.; Zhang, Y.; Deng, Z.; Ernst, K.-H.; Gao, H.-J. Polymorphism and Chiral Expression in Two-Dimensional Subphthalocyanine Crystals on Au(111). *Phys. Chem. Chem. Phys.* **2010**, *12*, 1318–1322.
57. Cun, H. Y.; Wang, Y. L.; Yang, B.; Zhang, L.; Du, S. X.; Wang, Y.; Ernst, K. H.; Gao, H. J. Homochiral Recognition among Organic Molecules on Copper(110). *Langmuir* **2010**, *26*, 3402–3406.
58. Fasel, R.; Parschau, M.; Ernst, K. H. Chirality Transfer from Single Molecules into Self-Assembled Monolayers. *Angew. Chem., Int. Ed.* **2003**, *42*, 5178–5181.
59. Wallach, O. *Liebigs Ann. Chem.* **1895**, *286*, 90–143.
60. Delley, B. From Molecules to Solids with the Dmol(3) Approach. *J. Chem. Phys.* **2000**, *113*, 7756–7764.
61. Perdew, J. P.; Wang, Y. Accurate and Simple Analytic Representation of the Electron-Gas Correlation-Energy. *Phys. Rev. B* **1992**, *45*, 13244–13249.
62. Delley, B. Hardness Conserving Semilocal Pseudopotentials. *Phys. Rev. B* **2002**, *66*, 155125.
63. *Accelrys*, 4.0 ed.; Accelrys Software Inc., 2009.